Published in "Journal of Cell Science 119: 2968-2974, 2006"
which should be cited to refer to this work.

Ablation of the single dynamin of *T. brucei* blocks mitochondrial fission and endocytosis and leads to a precise cytokinesis arrest

Anne-Laure Chanez[1], Adrian B. Hehl[2], Markus Engstler[3] and André Schneider[1,*]

[1]Department of Biology/Cell and Developmental Biology, University of Fribourg, Chemin du Musée 10, CH-1700 Fribourg, Switzerland
[2]Institute of Parasitology, University of Zurich, Winterthurerstr. 266a, CH-8057 Zurich, Switzerland
[3]Ludwig-Maximilians-Universität, Department Biologie I, Genetik, Maria-Ward-Str. 1a, München 80638, Germany
*Author for correspondence (e-mail: andre.schneider@unifr.ch)

Summary

Mitochondrial fission is mediated by dynamin-like proteins (DLPs). *Trypanosoma brucei* contains a single DLP, which is the only member of the dynamin superfamily. We have previously shown that expression of the human proapoptotic Bax in *T. brucei* induces extensive mitochondrial fragmentation. Here we report that Bax-induced mitochondrial fission is abolished in cell lines lacking functional DLP suggesting that the protein is also required for mitochondrial division during the cell cycle. Furthermore, DLP-ablated cells are deficient for endocytosis and as a consequence accumulate enlarged flagellar pockets. Thus, besides its expected role in mitochondrial fission the trypanosomal DLP is required for endocytosis, a function thought to be restricted to classical dynamins. In agreement with its dual function, the DLP localizes to both the mitochondrion and the flagellar pocket, the site where endocytosis occurs. Unexpectedly, ablation of DLP also causes an arrest of cytokinesis. The fact that no multinucleation is observed in the arrested cells argues for a precise cell-cycle block. Furthermore, analysis of a clathrin-knockdown cell line suggests that the cytokinesis arrest is not due to the endocytosis defect. Thus, our results support a working model in which mitochondrial fission triggers a checkpoint for cytokinesis.

Key words: Trypanosomes, Mitochondria, Endocytosis, Cell cycle

Introduction

Dynamin-like proteins (DLPs) are large modular GTPases consisting of the GTPase, the middle and the GTPase effector domains (Praefcke and McMahon, 2004). Together with the classical dynamins they define the eukaryotic superfamily of the dynamins. Classical dynamins in addition to the three modules found in DLPs also contain a pleckstrin-homology and a proline-rich domain. Whereas DLPs generally function in the division of organelles, such as mitochondria (Otsuga et al., 1998; Smirnova et al., 1998), chloroplasts (Gao et al., 2003; Miyagishima et al., 2003) and peroxisomes (Koch et al., 2003), classical dynamins are required for the scission of a wide range of vesicles including clathrin-coated pits in the secretory pathway (Hinshaw, 2000).

The genome of the parasitic protozoon *Trypanosoma brucei*, unlike most other eukaryotes, encodes only two tandemly linked, 97% identical DLPs (termed TbDLP), which are the sole members of the dynamin superfamily in this organism (Field and Carrington, 2004; Morgan et al., 2004). The two slightly different gene products are probably functionally equivalent, because the few amino acids that differ between them are spread over the entire length of the molecule and represent for the most part conservative substitutions.

T. brucei is ideally suited to study the mitochondrial-linked function of dynamins because it has a single mitochondrion (Tyler et al., 2001). Unlike the very dynamic mitochondria of mammalian cells (Scott et al., 2003), the *T. brucei* mitochondrion does not undergo any fission events throughout the cell cycle. Only before or during cytokinesis does the mitochondrion divide in two in order to allow its transmission to the daughter cells (McKean, 2003). Thus, in *T. brucei* mitochondrial fission must be coordinated with the cell cycle. Furthermore, *T. brucei* is also a good model to study the putative roles TbDLP might play in the secretory pathway. Endocytosis and exocytosis in *T. brucei* are known to be restricted to a small flask-shaped invagination of the plasma membrane containing the base of the flagellum, termed the flagellar pocket (FP) (Field and Carrington, 2004; Overath and Engstler, 2004). Furthermore, all intracellular endosomal compartments are found in a small region in the posterior part of the cell between the FP and the nucleus.

Endocytosis and mitochondrial activity are conversely regulated during the *T. brucei* life cycle. Bloodstream forms in the mammalian host show a ~tenfold higher endocytosis rate than the insect procyclic form (Engstler et al., 2005). Oxidative phosphorylation, on the other hand, is only essential in procyclic forms, which are characterized by having a large network-like single mitochondrion. The mitochondrion of bloodstream forms is much smaller, tube-like and not involved in ATP production (Schneider, 2001). In our work we were

concentrating on the procyclic form, which has the most active mitochondrion. The aim of our study was to investigate the involvement of TbDLP, the single dynamin of *T. brucei*, in mitochondrial fission and endocytosis. Moreover we wanted to test whether fission of the single *T. brucei* mitochondrion and cell division are independent of each other or whether there is a functional connection between the two events. Practically we approached the problem by inducible RNA interference (RNAi) or by regulated overexpression of a dominant-negative variant of the protein and subsequent analysis of the resulting cellular populations that lack functional TbDLP. The results showed that TbDLP is not only required for mitochondrial fission and endocytosis, but also for completion of cytokinesis.

Results

TbDLP is required for Bax-induced mitochondrial fission

Ablation of TbDLP in procyclic *T. brucei* by RNAi, in agreement with previously published work (Morgan et al., 2004), resulted in a growth arrest within 24 hours. However, unlike previous reports based on Mitotracker-stained cells, the mitochondrial morphology as analyzed by immunofluorescence appeared not to be significantly affected (Fig. 1A). It is known that in apoptotic human cells DLP is recruited by the proapoptotic Bax protein and that this results in extensive mitochondrial fragmentation (Bossy-Wetzel et al., 2003; Karbowski and Youle, 2003). Furthermore, we have previously shown that ectopic expression of human Bax induces mitochondrial fragmentation in *T. brucei* (Crausaz-Esseiva et al., 2004) (Fig. 1B). Thus, to test whether TbDLP is required for the Bax-induced mitochondrial fission, we constructed a cell line in which RNAi-mediated ablation of TbDLP was combined with Bax expression. Interestingly, the growth phenotype of this cell line (Fig. 1C) was essentially identical to the one of the TbDLP-RNAi cell line alone (Fig. 1A). Moreover, the proportion of cells showing mitochondrial fragmentation, which was 90% in the Bax-expressing cell line (Fig. 1B), became reduced to 14% (Fig. 1C). Bax-induced cytochrome *c* release, on the other hand, in agreement with our previous study (Crausaz-Esseiva et al., 2004), was still observed (data not shown). Very similar results were obtained for the cell line expressing the dominant-negative TbDLP (TbDLP-K39A), which is unable to hydrolyze GTP (Yoon et al., 2001) (see supplementary material Fig. S1). In summary, these results show that TbDLP – similarly to its mammalian homologue (Karbowski and Youle, 2003) – is required for Bax-induced mitochondrial fission and strongly suggest that it is also involved in the binary mitochondrial fission observed during cytokinesis.

TbDLP is required for endocytosis

TbDLP is the only member of the dynamin family in *T. brucei* (Morgan et al., 2004). This raises the question whether it might also be required for endocytosis. Indeed, analysis of TbDLP-ablated cells by light and electron microscopy shows an enlargement of the FP (Fig. 2A,B) a phenotype that is very similar to that caused by the ablation of clathrin heavy chain (CLH) (Engstler et al., 2005; Morgan et al., 2004) and actin (Garcia-Salcedo et al., 2004), two proteins known to be required for endocytosis in *T. brucei*. However, in these cases the enlarged FPs were reported to be restricted to the bloodstream stage, whereas in TbDLP-RNAi cells they are

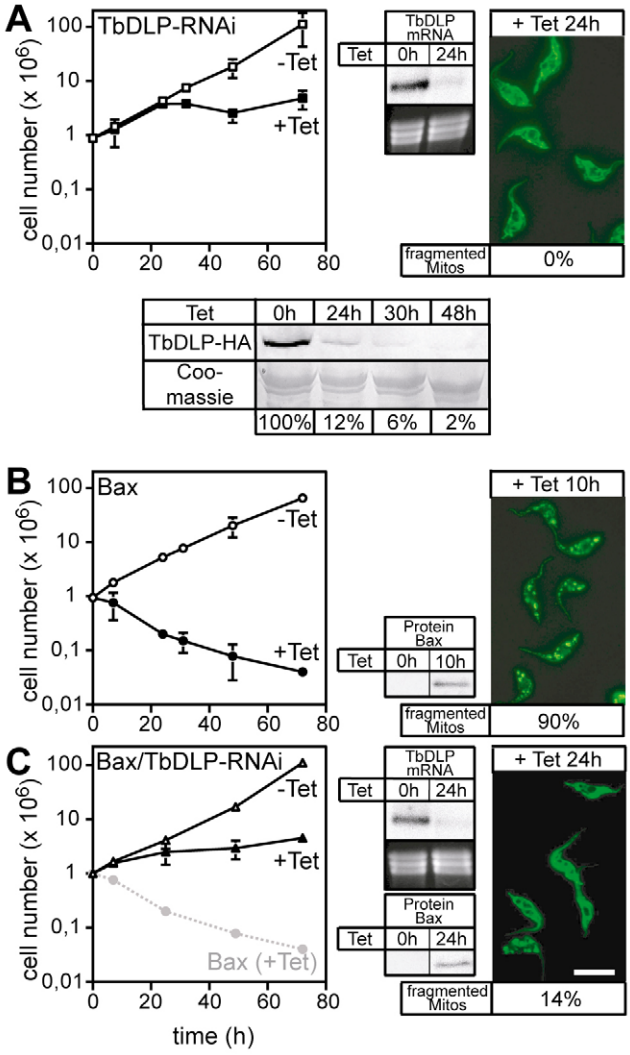

Fig. 1. TbDLP is required for Bax-induced mitochondrial fission. (A) Growth curve of the inducible (–Tet, +Tet) *T. brucei* TbDLP-RNAi cell line. RNAi was confirmed by northern blot (middle panel). Right panel: Immunofluorescence of induced cells using an inner mitochondrial membrane-specific F1-ATPase antiserum. The fraction of cells showing a fragmented mitochondrion is indicated. Bottom panel: Kinetics of TbDLP ablation tested by co-expression of a HA-tagged TbDLP (TbDLP-HA). The tagged protein was detected on immunoblots using anti HA-tag antiserum Y-11 (Santa Cruz Biotechnology). Hours of induction are indicated at the top. The lower half of the panel shows the Coomassie-stained tubulin region and serves as a loading control. (B) Same as A, but data are from a *T. brucei* cell line allowing inducible expression of human Bax (Crausaz-Esseiva et al., 2004). Bax expression was verified by immunoblot. (C) Same as A, but data are from a cell line allowing inducible expression of Bax and RNAi of TbDLP at the same time. The growth curve for the Bax-expressing cell line, as in B, is shown in grey for comparison. Standard errors (n=3-7) are indicated. Bar, 25 μm.

detected in procyclic cells. Concomitant with the appearance of the large FPs in 40-50% of induced TbDLP-RNAi cells, we observe a ~40% reduced endocytosis rate of fluorescently tagged surface proteins (Fig. 2C). Two-channel fluorescence microscopy, which allows the simultaneous scoring of enlarged

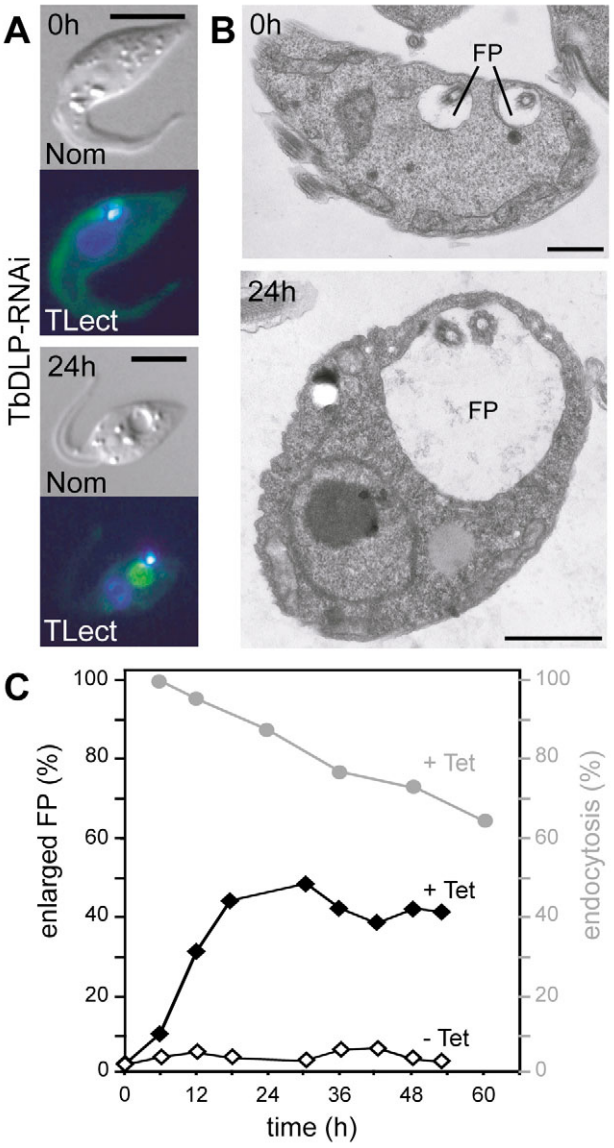

Fig. 2. TbDLP is required for endocytosis. (A) Ablation of TbDLP by RNAi results in enlarged FPs. FP in living cells were visualized by Fluorescein-conjugated tomato lectin (TLect). Nomarski (Nom) images and the merged pictures of the tomato lectin and the DAPI-staining of uninduced (0 h) and induced cells (24 h) are shown. Bars, 5 μm. (B), Analysis of the TbDLP-RNAi cell line by transmission electron microscopy. Bars, 1 μm. (C) Kinetics of appearance of enlarged FPs and loss of endocytic activity during induction of TbDLP-RNAi. FPs were visualized by AMCA sulfo-NHS labeling of surface proteins as described (Engstler et al., 2004). Enlarged FPs in uninduced (–Tet, ◇) and induced (+Tet, ◆) TbDLP-RNAi cells were automatically detected using a series of scripted digital image segmentation steps. Total endocytic activity was measured in the same culture by quantifying the internalized AMCA-labeled surface proteins (+Tet, grey symbols). All values were normalized to the corresponding total cell numbers (n>300 cells) and expressed relative to that of the corresponding uninduced culture.

FPs and endocytosis of a membrane dye within single cells, shows that 92.5±4.3% of cells with an enlarged FP were deficient for endocytosis, whereas the same was true for only 20.8±8.9% of cells having a normal FP. The TbDLP-K39A-expressing cell line exhibited an even stronger phenotype. Within 24 hours, 50% of the cells showed an enlarged FP and a 50% reduced uptake of labeled surface proteins (see supplementary material Fig. S2). Thus, in procyclic *T. brucei* a single DLP is required for both mitochondrial fission and endocytosis.

TbDLP shows a dual localization

To determine where in the cell TbDLP is localized we made use of epitope-tagged versions of the protein containing either an N-terminal or a C-terminal hemagglutinin (HA) tag. The results presented below are for the C-terminally tagged TbDLP. N-terminally tagged TbDLP gave the same results (data not shown). The genes encoding the tagged TbDLP proteins were integrated into their own genomic region in order to achieve expression as close as possible to natural levels (Shen et al., 2001). The resulting cell lines were analyzed by immunofluorescence in combination with confocal microscopy. As expected for a protein that is in part associated with the mitochondrial outer membrane TbDLP is detected in a punctate pattern that is associated but does not colocalize with the mitochondrial matrix marker Hsp60 (Fig. 3A). Furthermore, a strong TbDLP signal is detected next to the mitochondrial DNA. In *T. brucei* the highly concatenated mitochondrial genome, termed the kDNA, is not dispersed throughout the matrix but localized at a precise position opposite to the basal body of the flagellum and thus can easily be visualized by DAPI staining (McKean, 2003; Ogbadoyi et al., 2003). The localization of the kDNA-associated HA-tagged TbDLP was further analyzed by double staining with either the FP marker tomato lectin (Fig. 3B), the antibody YL1/2, which recognizes tyrosinated α-tubulin and serves as a marker for the basal body (Sherwin et al., 1987) (Fig. 3C), or antibodies against the flagellar attachment zone, a structure implicated in the cytokinesis (Kohl et al., 1999) (Fig. 3D). In summary these results show that the TbDLP is peripherally connected to the nucleus-facing side of the FP. It is closely associated but does not overlap with neither the basal body nor the flagellar attachment zone. Thus, in agreement with its dual function in mitochondrial fission and in endocytosis, TbDLP localizes to the mitochondrion (Fig. 3B) and the subregion of the FP where endocytosis is known to occur (Overath and Engstler, 2004) (Fig. 3E).

Lack of TbDLP leads to a precise arrest at the mid-cytokinesis stage

Unlike other eukaryotes, *T. brucei* has a distinct mitochondrial S phase that is initiated immediately before the onset of the longer nuclear S phase (McKean, 2003). Thus, segregation of the replicated kDNAs occurs before the onset of mitosis. The number of nuclei (N) and kDNAs (K) seen in DAPI-stained cells therefore allows us to determine three defined cell-cycle stages showing the 1K1N, 2K1N and 2K2N configurations. Interestingly, analysis of DAPI-stained TbDLP-RNAi cells shows a dramatic accumulation of 2K2N-cells indicative of a cytokinesis block. After 32 hours of induction the 2K2N-cells reach more than 4.5-fold the level (~45%) seen in the uninduced population (Fig. 4A). Most importantly, unlike in many other experiments where inhibition of cytokinesis was observed (Das et al., 1994; Kumar and Wang, 2006; LaCount et al., 2002), very few abnormal cells having configurations

other than 1K1N, 2K1N or 2K2N are detected (Fig. 4A, Others). Of the 2K2N-cells ~75% correspond to a subpopulation (Fig. 4A, NKKN subgroup), where the two kDNAs are localized between the two nuclei, a configuration which we termed NKKN (Fig. 4B, 4C lower panel and 4D). These cells have two opposed motile flagella (Fig. 4C) and resemble cell-cycle 'stage 10' (Sherwin and Gull, 1989) representing a late phase of cytokinesis, corresponding to two daughter cells that lay opposed to each other but which are still connected by their posterior parts. In a wild-type population NKKN cells represent <0.1% indicating that this cell cycle stage is very short. NKKN cells in the induced RNAi cell line, in agreement with the previously reported Mitotracker analysis (Morgan et al., 2004), consistently have a single continuous mitochondrion showing a more collapsed morphology than in uninduced cells (Fig. 4B). Furthermore NKKN cells always have two FPs (Fig. 4C), indicating that ablation of TbDLP does not impair the correct division of the FP. However, as expected from the endocytosis defect, at least one FP is enlarged. Fig. 4D shows that the organization of the flagellar attachment zone, which has been implicated in cytokinesis (Kohl et al., 1999), was not disturbed. Again these results were confirmed by using the TbDLP-K39A cell line (supplementary material Fig. S3).

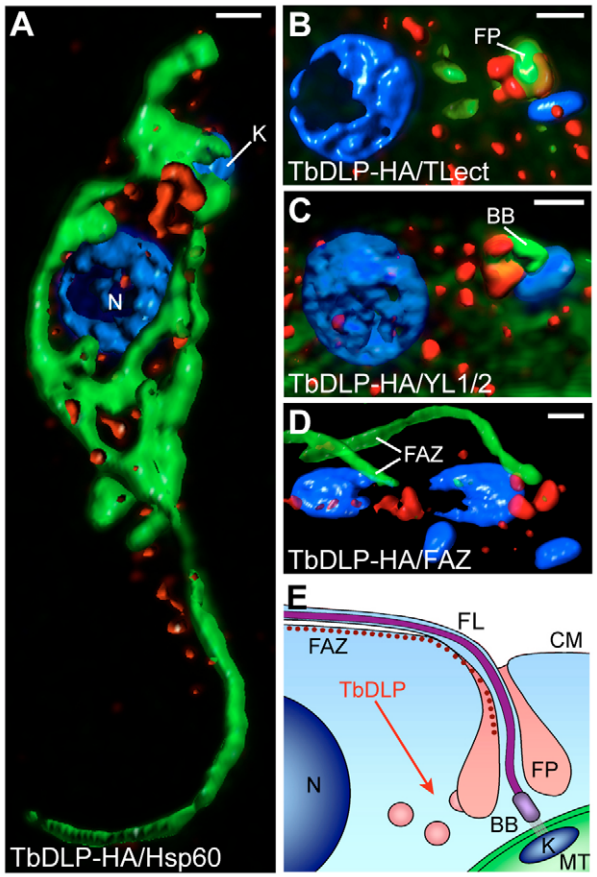

Fig. 3. TbDLP shows a dual localization. A transgenic *T. brucei* cell line expressing C-terminally HA-tagged TbDLP was analyzed by immunofluorescence. HA-tagged TbDLP was detected using anti HA-tag antiserum Y-11 (Santa Cruz Biotechnology) (red). Nuclear (N) and kDNA (K) were visualized by DAPI-staining (blue). The images show 3D-reconstructions from optical sections obtained by confocal microscopy. (A) Co-staining of HA-tagged TbDLP (red) with an antiserum recognizing Hsp60 (green), a marker protein for the mitochondrial matrix. (B) Same as A, but only the nucleus-kDNA region is shown and co-staining was done with the FP marker tomato lectin (TLect) (green). (C) Same as B, but co-staining was done with the antibody YL1/2 (green), which recognizes tyrosinated α-tubulin and serves as a marker for the basal body (BB) (Sherwin et al., 1987). (D) Same as B, but co-staining was done with the monoclonal mouse antibody L3B2 (shown in green), which recognizes the flagellar attachment zone (FAZ) (Kohl et al., 1999). (E) Schematic drawing of the nuclear-kDNA regions of *T. brucei*. The localization of the fraction of TbDLP that is required for endocytosis is indicated relative to intracellular structures and organelles. CM, cell membrane; FL, flagellum; FP, flagellar pocket; MT, mitochondrion. Bars, 1 μm.

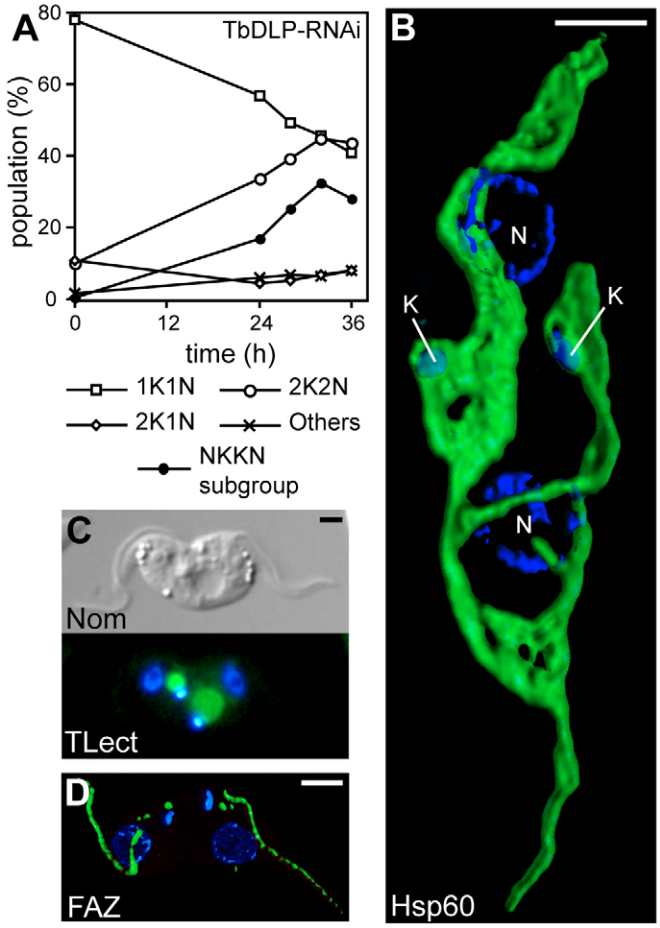

Fig. 4. Lack of TbDLP leads to a specific arrest of cytokinesis. (A) Analysis of nuclei and kDNA configurations of DAPI-stained cells during induction of TbDLP-RNAi. The graph indicates the percentages of cells containing the indicated numbers of nuclei and kDNAs (1K1N, 2K1N, 2K2N and others; *n*>1000 cells). Percentages of NKKN-cells, a subgroup of 2K2N cells where the two kDNAs are localized between the two nuclei, are also indicated. (B) NKKN-cells have a single mitochondrion. 3D-reconstruction from optical sections obtained by confocal microscopy of an anti-Hsp60 (green) and DAPI co-stained (blue) NKKN cell from the induced TbDLP-RNAi cell line. (C) NKKN cells have enlarged FPs. Visualization of FPs was done as in Fig. 2A. (D) Same as B, but staining was with the antibody L3B2 (green), which recognizes the flagellar attachment zone (FAZ) (Kohl et al., 1999). Bars, 2.5 μm.

Lack of clathrin impairs endocytosis but not cytokinesis

The two key components of the clathrin-mediated endocytosis pathway are dynamin and clathrin. Thus, ablation of clathrin is expected to mimic the endocytosis phenotype observed in the TbDLP-ablated cell lines. In agreement with this, it has been reported that RNAi-mediated depletion of clathrin heavy chain (CLH) in procyclic *T. brucei* causes a growth arrest and a block of endocytosis (Allen et al., 2003; Hung et al., 2004). Exocytosis however was, except for the export of the FP-localized receptor CRAM (Hung et al., 2004), not affected. Thus, in order to test whether endocytosis deficiency can lead to a cytokinesis arrest, we prepared a TbCLH-RNAi cell line. As expected, these cells showed a growth arrest (Fig. 5A) and a reduction of endocytosis (Fig. 5B) after induction of RNAi. However, unlike results described before, concomitant with the growth arrest and in line with the endocytosis defect, we observed that up to 25% of the cells had an enlarged FP (Fig. 5B). Most importantly, even though the enlarged FP and the deficient endocytosis are features also observed in the TbDLP-RNAi cell line, ablation of CLH at no time caused the accumulation of 2K2N cells (Fig. 5C). Thus, the lack of endocytosis or an enlarged FP cannot explain the cytokinesis phenotype caused by the inactivation of TbDLP (Fig. 4A).

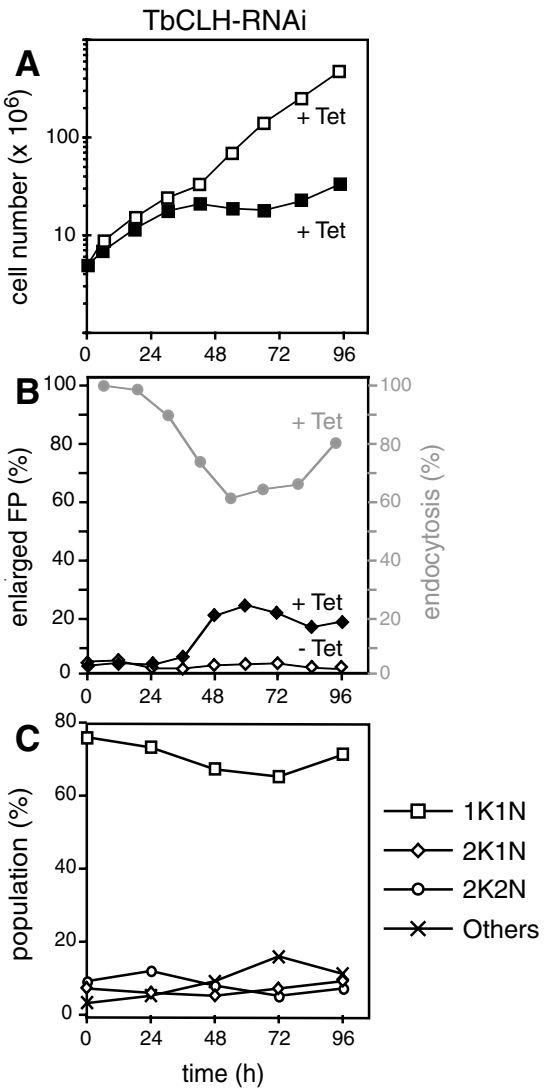

Fig. 5. Lack of TbCLH impairs endocytosis but not cytokinesis. (A) Growth curve of the uninduced and induced TbCLH-RNAi cell line. (B) Kinetics of appearance of enlarged FPs and loss of endocytic activity during induction of TbCLH-RNAi. Analysis was performed as in Fig. 2C. (C) Analysis of nuclei and kDNA configurations of DAPI-stained cells during induction of TbCLH-RNAi carried out as in Fig. 4A.

Discussion

Our results show that TbDLP is required for both mitochondrial fission and – contrary to an earlier report (Morgan et al., 2004) – for endocytosis. At present we cannot explain this discrepancy, but it is interesting to note that the RNAi strategy that was used in our study was based on the expression of a stem-loop RNA whereas in the previous study (Morgan et al., 2004) the two RNA strands were expressed from a single DNA fragment using two opposing T7 promoters. With the stem-loop construct maximal depletion is reached after 1-2 days (Fig. 1A), whereas in the RNAi cell lines produced by Morgan et al. minimal TbDLP levels are reached after 3-4 days. Thus, some of the differences between the results of two studies might be due to the different kinetics and extent of TbDLP depletion. However, it is important to emphasize that whereas the previous study was based on RNAi only, we inactivated TbDLP by either RNAi or expression of the dominant-negative TbDLP-K39A and obtained the same phenotypes. Thus, our results show that clathrin-mediated endocytosis, which generally requires a classical dynamin (Hinshaw, 2000), can be mediated by a DLP suggesting that to some extent classical dynamins and DLPs are functionally interchangeable. Classical dynamins are essentially restricted to metazoans whereas DLPs occur in all eukaryotes. This suggests that DLPs are the most ancestral members of the dynamin superfamily (Elde et al., 2005). *T. brucei* is one of the earliest diverging eukaryotes with a bona fide mitochondrion and its single DLP is required for mitochondrial fission and endocytosis. The unrelated parasitic protozoon *Giardia* branches off the eukaryotic evolutionary tree even earlier, it does not have mitochondria but contains mitochondrial remnant organelles lacking DNA (Tovar et al., 2003), termed mitosomes. Similar to trypanosomes *Giardia* contains a single DLP. Recent experiments have shown that this protein is required for endocytosis, but not for the division of mitosomes (A.H., unpublished results). Thus, these results suggest that the ancestral function of DLPs might have been in endocytosis.

TbDLP-ablated cells are also deficient in cytokinesis. Could it be that TbDLP, besides its role in mitochondrial fission and in endocytosis, has a third function and is directly involved in cell division? We find this unlikely because high-resolution confocal microscopy in dividing 2K2N cells failed to reveal any colocalization of TbDLP with the cleavage furrow (e.g. Fig. 3D and data not shown). Furthermore, it is known that the controls of mitosis and cytokinesis are dissociated in procyclic *T. brucei* and that the mitosis-to-cytokinesis checkpoint, which is operational in mammalian cells, is absent (Das et al., 1994; Kumar and Wang, 2006; LaCount et al., 2002; McKean, 2003; Robinson et al., 1995). Inhibition of cytokinesis therefore invariably causes the appearance of cells having multiple nuclei (Das et al., 1994; LaCount et al., 2002). Inactivation of TbDLP, however, leads to a precise cell-cycle arrest without

appearance of multinucleated cells (Fig. 4A, supplementary material Fig. S3A) providing a further argument against a direct role of TbDLP in cytokinesis.

Analysis of CLH-ablated cells reproduced the same endocytosis defect observed in cells devoid of functional TbDLP but did not cause a cell-cycle phenotype (Fig. 5). This indicates that the cytokinesis phenotype is linked to the defect in mitochondrial fission. A trivial explanation for this would be that the undivided mitochondrion blocks cytokinesis mechanically. We find this unlikely because, in contrast to what would be expected in this case, no central constriction caused by the blocked cleavage furrow is observed in the NKKN cells (Fig. 4C and supplementary material Fig. S3C, upper panel). Moreover, as discussed above, mechanical blockage of cytokinesis would almost certainly cause accumulation of multinucleated cells (Das et al., 1994; LaCount et al., 2002). This is not seen (Fig. 4A and supplementary material Fig. S3A). In fact our results are reminiscent of the block of cytokinesis observed in a bloodstream *T. brucei* cell line ablated for the variable surface glycoprotein (VSG) (Sheader et al., 2005), because multinucleated cells did not accumulate in this case either. It has been suggested, that the observed pre-cytokinesis arrest in this cell line is due to a cell-cycle checkpoint, the function of which would be to coordinate VSG synthesis with cell division (Sheader et al., 2005). Thus, analogous to this interpretation, we propose a model in which inhibition of mitochondrial fission by inactivation of TbDLP prevents completion of cytokinesis by triggering a cell-cycle checkpoint. We think that such a model makes biological sense because the mitochondrial genome of *T. brucei* is of a one-unit nature and because cytokinesis is uncoupled from mitosis (Kumar and Wang, 2006; McKean, 2003; Ploubidou et al., 1999; Robinson et al., 1995). This strongly suggests that novel cell-cycle checkpoints are indeed required. Recent work provides evidence that one of these might be linked to the segregation of the replicated kDNAs (McKean, 2003; Ploubidou et al., 1999). In our model we propose that mitochondrial fission may serve as a checkpoint acting further downstream whose function would be to prevent the production of daughter cells lacking a kDNA or a mitochondrion altogether.

A cell line ablated for Fis1, a protein uniquely involved in mitochondrial fission which acts in concert with DLP (Scott et al., 2003), would in principle be an excellent tool to confirm our results. We did indeed find a putative Fis1 orthologue in the *T. brucei* genomic database. However unfortunately, owing to inefficient RNAi, ablation of the trypanosomal Fis1 was not possible.

Our work shows that in *T. brucei*, TbDLP function links mitochondrial fission, endocytosis and cytokinesis. We believe that the most parsimonious explanation for these results is the existence of a checkpoint for the completion of cytokinesis that monitors mitochondrial fission. However, since alternative explanations cannot entirely be excluded, this must remain a working model at present. Interestingly, some connections of DLPs with cell-cycle progression have been described in other systems. In *Dictyostelium discoideum* a null mutant of an unconventional DLP (DymA) shows pleiotropic defects, one of which concerns the completion of cytokinesis (Wienke et al., 1999). However, unlike in *T. brucei*, the observed cytokinesis arrest was accompanied by the appearance of multinucleated cells and therefore is inconsistent with a specific cell-cycle arrest. RNAi-mediated ablation of the DLP homologue of *Caenorhabditis elegans*, on the other hand, causes embryonic lethality (Labrousse et al., 1999), a result that would be consistent with a mitochondrial segregation defect.

Materials and Methods

Production of transgenic cell lines

TbDLP-RNAi was performed using a stem-loop construct containing the puromycin-resisitant gene as described (Bochud-Allemann and Schneider, 2002). A 502 bp fragment of the TbDLP gene corresponding to nucleotides 1251-1753 was used as an insert. To produce the Bax/TbDLP-RNAi cell line the previously described Bax-expressing cells (Crausaz-Esseiva et al., 2004) selected using phleomycin were transfected with the TbDLP-RNAi plasmid and transfectants were then selected using puromycin and phleomycin. Inducible overexpression of wild-type TbDLP and TbDLP-K39A (where Lys39 was replaced with Ala) was based on the same plasmids used for RNAi. The inducible TbCLH-RNAi cell line was produced by using the construct described by Engstler et al. (Engstler et al., 2005). To produce epitope-tagged variants of TbDLP the recently described one-step PCR-based strategy was used (Shen et al., 2001). Cells were grown in SDM-79 supplemented with 5% (for the 427 strain, used for epitope tagging) or 15% FCS (for 29-13 strain, used for RNAi and overexpression of proteins) and the required antibiotic(s). Transfection, selection with antibiotics, cloning and induction with tetracycline were done as described (McCulloch et al., 2004).

Endocytosis assays

The FPs were analyzed by fluorescence microscopy by labeling with 10 mg/ml Fluorescein-conjugated tomato lectin (Vector Laboratories) (Fig. 2A, Fig. 3B, Fig. 4C and supplementary material Fig. S2A, Fig. S3C). Alternatively, FPs were also visualized by labeling of surface proteins using 1 mM AMCA-sulfo-NHS (Pierce) (Fig. 2C, Fig. 5B and supplementary material Fig. S2B) and incubation for 10 minutes at 0°C followed by 30 minutes at 27°C. Subsequently, after a washing step and fixation of the cells in 4% paraformaldehyde, the FPs were visualized by AMCA fluorescence. It was previously shown that fluorescence of the internalized AMCA-labeled proteins is quantitatively quenched, thus AMCA fluorescence selectively detects labeled proteins on the cell surface and in the FP (Engstler et al., 2004). Enlarged FPs were automatically scored using a series of scripted digital image segmentation steps. This allowed us to determine the fraction of cells at the indicated time points having at least one enlarged FP (Fig. 2C, black curves and supplementary material Fig. S2B, black curves).

To measure endocytosis, surface proteins were labeled with AMCA-sulfo-NHS and incubated as decribed above. Subsequently, AMCA-labeled surface proteins and AMCA-labeled internalized proteins were detected in fixed and permeabilized cells using a rabbit anti-AMCA antibody and an Alexa Fluor 594-conjugated secondary antibody. Cells having internalized AMCA were scored and for each time point the fraction of the total cellular population showing internalized AMCA fluorescence was determined (Fig. 2C, grey curve and supplementary material Fig. S2B, grey curve). Alternatively, endocytosis was measured in living cells by assaying the uptake of the fluorescent membrane dye FM1-43FX (Molecular Probes). AMCA-labeled cells were incubated in the presence of the fluorescent probe for 30 minutes at 27°C, washed with ice-cold PBS and fixed with 4% paraformaldehyde and 0.5% glutaraldehyde. The washing step removes the dye from the plasma membrane and the FP, whereas endocytosed FM1-43FX is retained in endosomal membranes and can be fixed. Two-channel fluorescence microscopy allows the simultaneous scoring for normal or enlarged FPs and internalized FM1-43FX in single cells.

Immunofluorescence and confocal microscopy

Immunofluorescence was performed as described (Sherwin et al., 1987). Fixation was done using 4% (w/v) paraformaldehyde in PBS for 10 minutes and cells were permeabilized for 2 minutes using PBS containing 2% (w/v) Triton X-100. Mitochondrial morphology was assessed by a 1:200 dilution of a polyclonal rabbit anti-F1-ATPase antiserum (gift from D. Speijer, AMC, Amsterdam, The Netherlands) raised against the isolated mitochondrial ATPase of *Crithidia fasciculata* (Fig. 1 and supplementary material Fig. S1) or with 1:1000 dilution of a mouse polyclonal anti-Hsp60 antiserum, raised against recombinantly expressed *T. brucei* Hsp60 fused to gluthathione S-transferase (Fig. 3A, Fig. 4B and supplementary material Fig. S3). Cells were washed with PBS between incubations, and embedded with Vectashield (Vector Labs, Emeryville, CA) supplemented with the DNA-intercalating agent DAPI for detection of nuclear DNA. Fluorescence analysis (Fig. 3, Fig. 4B and supplementary material Fig. S2B) was performed on a Leica SP2 AOBS confocal laser-scanning microscope (Leica Microsystems, Wetzlar, Germany) using a HCX PL APO (63× /1.3 Glyc Corr) objective and the appropriate laser and photo multiplier settings. Image stacks of 512×512 pixels

were collected using twofold oversampling and further processed using the Leica software, the Huygens Essential deconvolution package (Scientific Volume Imaging, Hilversum, The Netherlands) or Imaris (Bitplane, Zurich, Switzerland). Thresholds for isosurface analysis were calculated automatically and adapted to specific structures manually based on the volume image.

We thank E. Horn, L. Bulliard, A. Hemphill and M. Schorderet for technical assistence. Furthermore we thank G. Cross, P. Englund, K. Gull, D. Speijer and C. Tschudi for providing us with cell lines, plasmids and antisera. We acknowledge many helpful suggestions from E. Vassella. This work was supported by grants 3100-067906 (A.S.) and 3100A0-100270 (A.H.) of the Swiss National Foundation as well as by grant EN305-2 (M.E.) of the DFG.

References

Allen, C. L., Goulding, D. and Field, M. C. (2003). Clathrin-mediated endocytosis is essential in *Trypanosoma brucei*. *EMBO J.* **22**, 4991-5002.

Bochud-Allemann, N. and Schneider, A. (2002). Mitochondrial substrate level phosphorylation is essential for growth of procyclic *Trypanosoma brucei*. *J. Biol. Chem.* **277**, 32849-32854.

Bossy-Wetzel, E., Barsoum, M. J., Godzik, A., Schwarzenbacher, R. and Lipton, S. A. (2003). Mitochondrial fission in apoptosis, neurodegeneration and aging. *Curr. Opin. Cell Biol.* **15**, 706-716.

Crausaz-Esseiva, A., Chanez, A.-L., Bochud-Allemann, N., Martinou, J. C., Hemphill, A. and Schneider, A. (2004). Temporal dissection of Bax-induced events leading to fission of the single mitochondrion in *Trypanosoma brucei*. *EMBO Rep.* **5**, 268-273.

Das, A., Gale, M., Carter, V. and Parsons, M. (1994). The protein phosphatase inhibitor okadaic acid induces defects in cytokinesis and organellar genome segregation in *Trypanosoma brucei*. *J. Cell Sci.* **107**, 3477-3483.

Elde, N. C., Morgan, G., Winey, M., Sperling, L. and Turkewitz, A. P. (2005). Elucidation of clathrin-mediated endocytosis in tetrahymena reveals an evolutionarily convergent recruitment of dynamin. *PLoS Genet.* **1**, e52.

Engstler, M., Thilo, L., Weise, F., Grunfelder, C. G., Schwarz, H., Boshart, M. and Overath, P. (2004). Kinetics of endocytosis and recycling of the GPI-anchored variant surface glycoprotein in *Trypanosoma brucei*. *J. Cell Sci.* **117**, 1105-1115.

Engstler, M., Weise, F., Bopp, K., Grunfelder, C. G., Gunzel, M., Heddergott, N. and Overath, P. (2005). The membrane-bound histidine acid phosphatase TbMBAP1 is essential for endocytosis and membrane recycling in *Trypanosoma brucei*. *J. Cell Sci.* **118**, 2105-2118.

Field, M. C. and Carrington, M. (2004). Intracellular membrane transport systems in *Trypanosoma brucei*. *Traffic* **5**, 905-913.

Gao, H., Kadirjan-Kalbach, D., Froehlich, J. E. and Osteryoung, K. W. (2003). ARC5, a cytosolic dynamin-like protein from plants, is part of the chloroplast division machinery. *Proc. Natl. Acad. Sci. USA* **100**, 4328-4333.

Garcia-Salcedo, J. A., Perez-Morga, D., Gijon, P., Dilbeck, V., Pays, E. and Nolan, D. P. (2004). A differential role for actin during the life cycle of *Trypanosoma brucei*. *EMBO J.* **23**, 780-789.

Hinshaw, J. E. (2000). Dynamin and its role in membrane fission. *Annu. Rev. Cell Dev. Biol.* **16**, 483-519.

Hung, C. H., Qiao, X., Lee, P. T. and Lee, M. G. (2004). Clathrin-dependent targeting of receptors to the flagellar pocket of procyclic-form *Trypanosoma brucei*. *Eukaryotic Cell* **3**, 1004-1014.

Karbowski, M. and Youle, R. J. (2003). Dynamics of mitochondrial morphology in healthy cells and during apoptosis. *Cell Death Differ.* **10**, 870-880.

Koch, A., Thiemann, M., Grabenbauer, M., Yoon, Y., McNiven, M. A. and Schrader, M. (2003). Dynamin-like protein 1 is involved in peroxisomal fission. *J. Biol. Chem.* **278**, 8597-8605.

Kohl, L., Sherwin, T. and Gull, K. (1999). Assembly of the paraflagellar rod and the flagellum attachment zone complex during the *Trypanosoma brucei* cell cycle. *J. Eukaryot. Microbiol.* **46**, 105-109.

Kumar, P. and Wang, C. C. (2006). Dissociation of cytokinesis initiation from mitotic control in a eukaryote. *Eukaryotic Cell* **5**, 92-102.

Labrousse, A. M., Zappaterra, M. D., Rube, D. A. and van der Bliek, A. M. (1999). *C. elegans* dynamin-related protein DRP-1 controls severing of the mitochondrial outer membrane. *Mol. Cell* **4**, 815-826.

LaCount, D. J., Barrett, B. and Donelson, J. E. (2002). *Trypanosoma brucei* FLA1 is required for flagellum attachment and cytokinesis. *J. Biol. Chem.* **277**, 17580-17588.

McCulloch, R., Vassella, E., Burton, P., Boshart, M. and Barry, J. D. (2004). Transformation of monomorphic and pleomorphic *Trypanosoma brucei*. *Methods Mol. Biol.* **262**, 53-86.

McKean, P. G. (2003). Coordination of cell cycle and cytokinesis in *Trypanosoma brucei*. *Curr. Opin. Microbiol.* **6**, 600-607.

Miyagishima, S. Y., Nishida, K., Mori, T., Matsuzaki, M., Higashiyama, T., Kuroiwa, H. and Kuroiwa, T. (2003). A plant-specific dynamin-related protein forms a ring at the chloroplast division site. *Plant Cell* **15**, 655-665.

Morgan, G. W., Goulding, D. and Field, M. C. (2004). The single dynamin-like protein of *Trypanosoma brucei* regulates mitochondrial division and is not required for endocytosis. *J. Biol. Chem.* **279**, 10692-10701.

Ogbadoyi, E. O., Robinson, D. R. and Gull, K. (2003). A high-order trans-membrane structural linkage is responsible for mitochondrial genome positioning and segregation by flagellar basal bodies in trypanosomes. *Mol. Biol. Cell* **14**, 1769-1779.

Otsuga, D., Keegan, B. R., Brisch, E., Thatcher, J. W., Hermann, G. J., Bleazard, W. and Shaw, J. M. (1998). The dynamin-related GTPase, Dnm1p, controls mitochondrial morphology in yeast. *J. Cell Biol.* **143**, 333-349.

Overath, P. and Engstler, M. (2004). Endocytosis, membrane recycling and sorting of GPI-anchored proteins: *Trypanosoma brucei* as a model system. *Mol. Microbiol.* **53**, 735-744.

Ploubidou, A., Robinson, D. R., Docherty, R. C., Ogbadoyi, E. O. and Gull, K. (1999). Evidence for novel cell cycle checkpoints in trypanosomes: kinetoplast segregation and cytokinesis in the absence of mitosis. *J. Cell Sci.* **112**, 4641-4650.

Praefcke, G. J. and McMahon, H. T. (2004). The dynamin superfamily: universal membrane tubulation and fission molecules? *Nat. Rev. Mol. Cell Biol.* **5**, 133-147.

Robinson, D. R., Sherwin, T., Ploubidou, A., Byard, E. H. and Gull, K. (1995). Microtubule polarity and dynamics in the control of organelle positioning, segregation, and cytokinesis in the trypanosome cell cycle. *J. Cell Biol.* **128**, 1163-1172.

Schneider, A. (2001). Unique aspects of mitochondrial biogenesis in trypanosomatids. *Int. J. Parasitol.* **31**, 1403-1415.

Scott, S. V., Cassidy-Stone, A., Meeusen, S. L. and Nunnari, J. (2003). Staying in aerobic shape: how the structural integrity of mitochondria and mitochondrial DNA is maintained. *Curr. Opin. Cell Biol.* **15**, 482-488.

Sheader, K., Vaughan, S., Minchin, J., Hughes, K., Gull, K. and Rudenko, G. (2005). Variant surface glycoprotein RNA interference triggers a precytokinesis cell cycle arrest in African trypanosomes. *Proc. Natl. Acad. Sci. USA* **102**, 8716-8721.

Shen, S., Arhin, G. K., Ullu, E. and Tschudi, C. (2001). In vivo epitope tagging of *Trypanosoma brucei* genes using a one step PCR-based strategy. *Mol. Biochem. Parasitol.* **113**, 171-173.

Sherwin, T. and Gull, K. (1989). The cell division cycle of *Trypanosoma brucei brucei*: timing of event markers and cytoskeletal modulations. *Philos. Trans. R. Soc. Lond. B Biol. Sci.* **323**, 573-588.

Sherwin, T., Schneider, A., Sasse, R., Seebeck, T. and Gull, K. (1987). Distinct localization and cell cycle dependence of COOH terminally tyrosinolated a-tubulin in the microtubules of *Trypanosoma brucei* brucei. *J. Cell Biol.* **104**, 439-445.

Smirnova, E., Shurland, D. L., Ryazantsev, S. N. and van der Bliek, A. M. (1998). A human dynamin-related protein controls the distribution of mitochondria. *J. Cell Biol.* **143**, 351-358.

Tovar, J., Leon-Avila, G., Sanchez, L. B. and Sutak, R. (2003). Mitochondrial remnant organelles of Giardia function in iron-sulphur protein maturation. *Nature* **426**, 127-128.

Tyler, K. M., Matthews, K. R. and Gull, K. (2001). Anisomorphic cell division by African trypanosomes. *Protist* **152**, 367-378.

Wienke, D. C., Knetsch, M. L., Neuhaus, E. M., Reedy, M. C. and Manstein, D. J. (1999). Disruption of a dynamin homologue affects endocytosis, organelle morphology, and cytokinesis in *Dictyostelium discoideum*. *Mol. Biol. Cell* **10**, 225-243.

Yoon, Y., Pitts, R. K. and McNiven, M. A. (2001). Mammalian dynamin-like protein DLP1 tubulates membranes. *Mol. Biol. Cell* **12**, 2894-2905.

Fig. S1. Expression of the dominant-negative TbDLP (TbDLP-K39A) inhibits Bax-induced mitochondrial fission. **(A)** Growth curve of a *T. brucei* cell line allowing inducible overexpression of TbDLP. **(B))** *T. brucei* cell line allowing inducible expression of TbDLP-K39A. **(C)** Cell line allowing inducible coexpression of Bax and TbDLP-K39A. Expression of Bax was verified by immunoblot. The growth curve for the Bax-expressing cell line (as in Fig. 1B), is shown in grey for comparison. Right panels, immunofluorescence as in Fig. 1. Standard errors (*n*=3-7) are indicated. Bar, 25 μm.

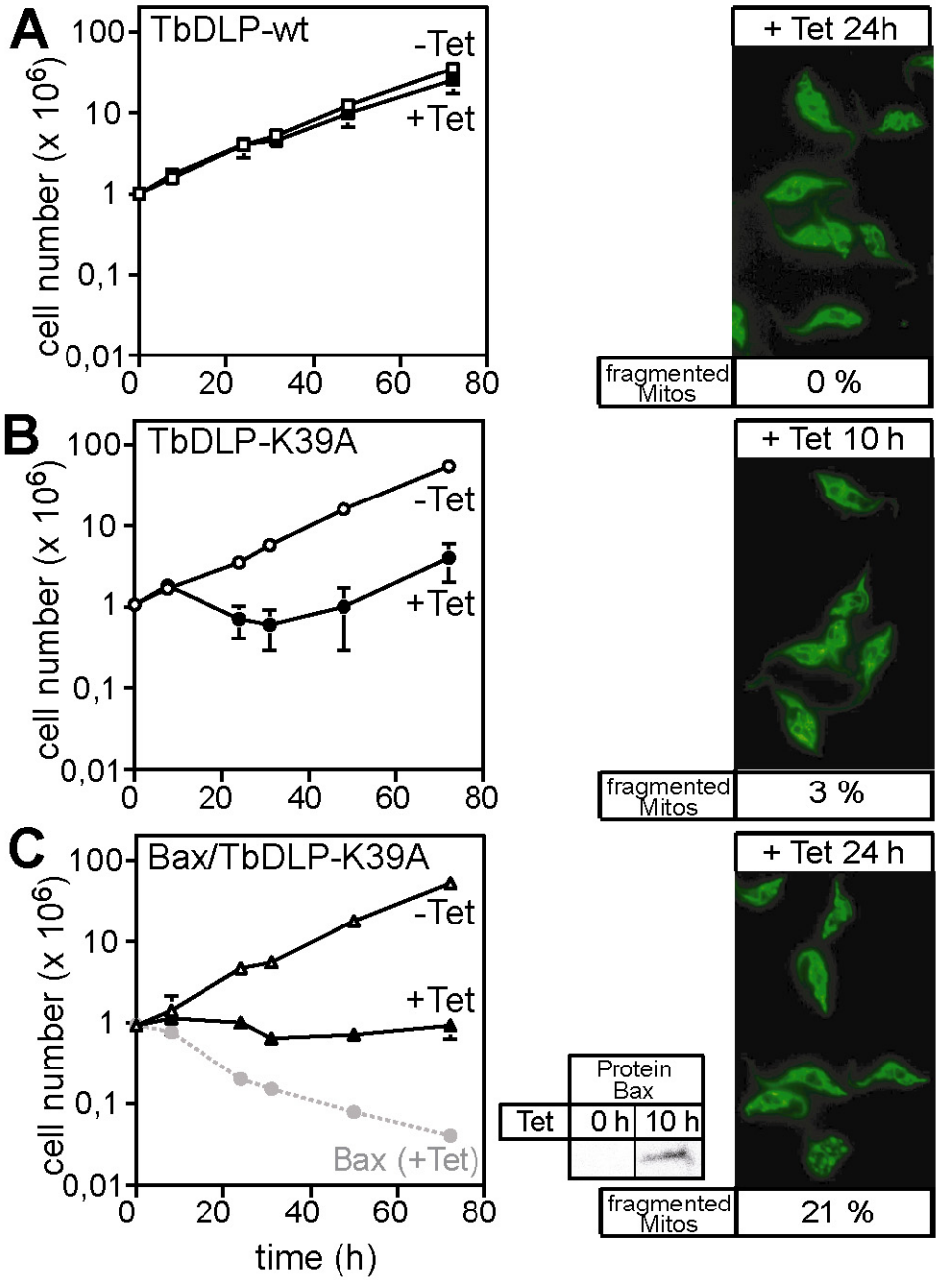
A
TbDLP-wt
-Tet
+Tet
cell number (x 10^6)
100
10
1
0,1
0,01
0
20
40
60
80
+ Tet 24h
fragmented Mitos
0 %
B
TbDLP-K39A
-Tet
+Tet
cell number (x 10^6)
+ Tet 10 h
fragmented Mitos
3 %
C
Bax/TbDLP-K39A
-Tet
+Tet
Bax (+Tet)
cell number (x 10^6)
time (h)
Protein Bax
Tet
0 h
10 h
+ Tet 24 h
fragmented Mitos
21 %

Fig. S2. Expression of the dominant TbDLP-K39A inhibits endocytosis. (A) Overexpression of TbDLP-K39A results in enlarged FPs. FPs in living cells were visualized by fluorescein-conjugated tomato lectin (TLect). Nomarski (Nom) images and the merged images of the tomato lectin and the DAPI-staining of uninduced (0 h) and induced cells (14 h). Bars, 5 μm. (B) Kinetic of appearance of enlarged FPs and loss of endocytic activity after induction of TbDLP-K39A expression. Visualization of the FP in uninduced and induced cells was done by AMCA sulfo-NHS labeling of surface proteins as described (Engstler et al., 2004). Enlarged flagellar pockets in uninduced (–Tet, white diamonds) and induced (+Tet, black diamonds) TbDLP-K39A-expressing cells were automatically detected using a series of scripted digital image segmentation steps. Total endocytic activity was measured in the same culture by quantifying the internalized AMCA-labeled surface proteins (+Tet, grey symbols). All values were normalized to the corresponding total cell numbers (n>300 cells) and expressed relative to the one of the corresponding uninduced cultures. Single-cell analysis showed that 89.8±6.2% of cells having an enlarged FP were defective in endocytosis, whereas 87.4±7.6% of cells with a normal FP showed normal endocytic activity.

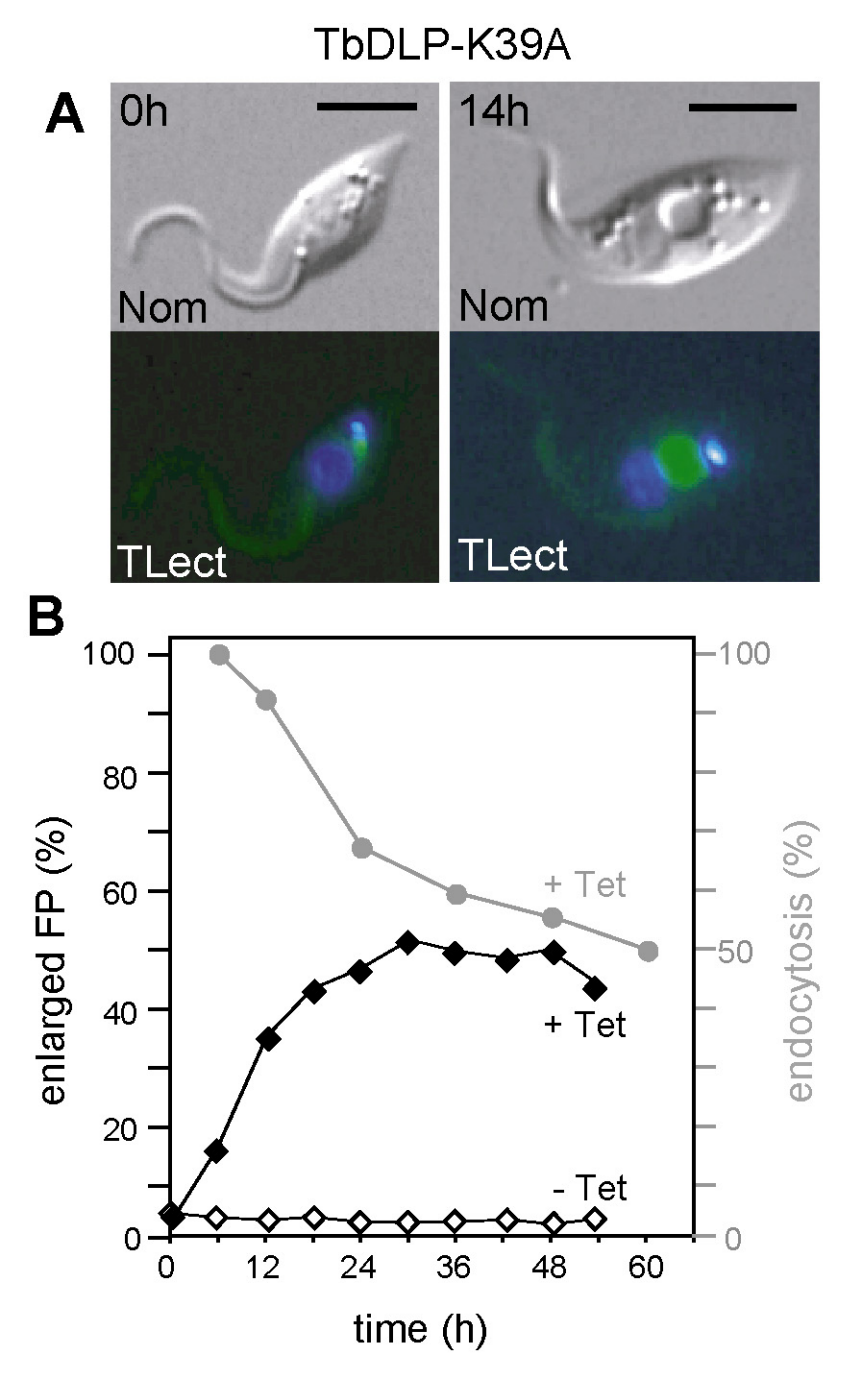
TbDLP-K39A
A
0h
14h
Nom
Nom
TLect
TLect
B
100
80
60
40
20
0
enlarged FP (%)
100
50
0
endocytosis (%)
+ Tet
+ Tet
- Tet
0
12
24
36
48
60
time (h)

Legend Fig. S3.

Fig. S3. Expression of the dominant TbDLP-K39A leads to a specific arrest of cytokinesis. (A) Analysis of nuclei and kDNA configurations of DAPI-stained cells during induction of TbDLP-K39A expression. The graph indicates the percentages of cells containing the indicated numbers of nuclei and kDNAs (1K1N, 2K1N, 2K2N and others; *n*>1000 cells). Percentages of NKKN cells. A subgroup of 2K2N cells where the two kDNAs are localized between the two nuclei, is also indicated. (B) NKKN cells have a single mitochondrion. 3D reconstruction from optical sections obtained by confocal microscopy of an anti-Hsp60 (green) and DAPI co-stained (blue) NKKN cell from the TbDLP-K39A-expressing cell line. (C) NKKN cells have enlarged FPs. Visualization of the FPs was as described in Fig. 2A. Bars, 2.5 μm.Fig. S3. Expression of the dominant TbDLP-K39A leads to a specific arrest of cytokinesis. (A) Analysis of nuclei and kDNA configurations of DAPI-stained cells during induction of TbDLP-K39A expression. The graph indicates the percentages of cells containing the indicated numbers of nuclei and kDNAs (1K1N, 2K1N, 2K2N and others; n>1000 cells). Percentages of NKKN cells. A subgroup of 2K2N cells where the two kDNAs are localized between the two nuclei, is also indicated. (B) NKKN cells have a single mitochondrion. 3D reconstruction from optical sections obtained by confocal microscopy of an anti-Hsp60 (green) and DAPI co-stained (blue) NKKN cell from the TbDLP-K39A-expressing cell line. (C) NKKN cells have enlarged FPs. Visualization of the FPs was as described in Fig. 2A. Bars, 2.5 μm.

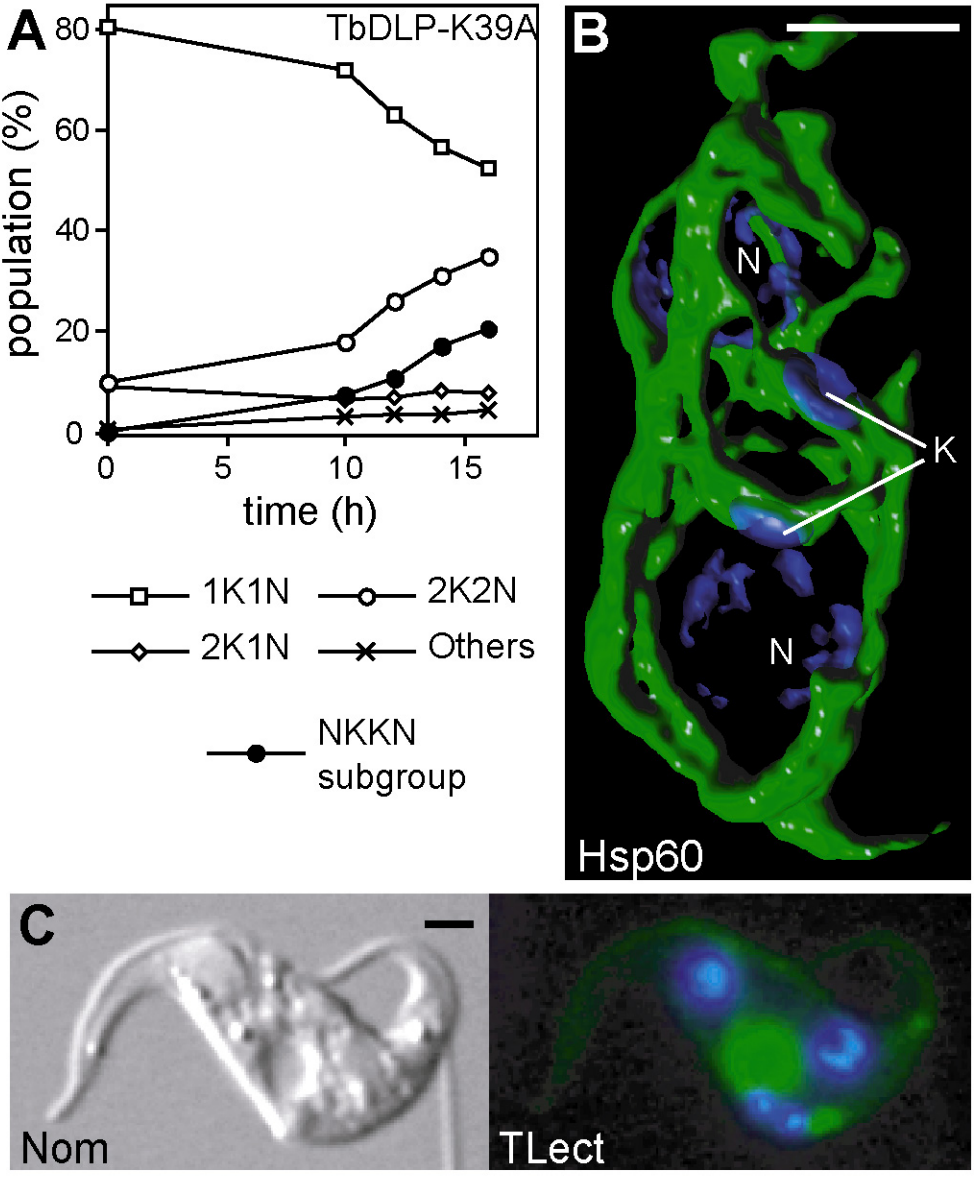
A
TbDLP-K39A
population (%)
80
60
40
20
0
0
5
10
15
time (h)
1K1N
2K2N
2K1N
Others
NKKN
subgroup
B
N
K
N
Hsp60
C
Nom
TLect